PROCEEDINGS, 42nd Workshop on Geothermal Reservoir Engineering
Stanford University, Stanford, California, February 13-15, 2017
SGP-TR-212

Experimental Investigation of Injection-driven Shear Slip and Permeability Evolution in Granite for EGS Stimulation

Zhi Ye[1], Michael Janis[1], Ahmad Ghassemi[1], Stephen Bauer[2]

1. Reservoir Geomechanics and Seismicity Research Group, The University of Oklahoma, Norman, OK 73069;

2. Sandia National Laboratories, Albuquerque, NM 87123

ahmad.ghassemi@ou.edu

Keywords: fluid injection-driven shear slip, hydroshearing, tensile rough fracture, permeability evolution, EGS

ABSTRACT

Permeability enhancement through shear slip has been considered as standard treatment of engineered geothermal systems (EGS). The so-called "hydroshearing" process reactivates pre-existing fractures to slip and dilate using fluid pressures below the minimum principal stress and can also cause fracture propagation in the shear and tensile modes creating secondary cracks, resulting in increased permeability for economic flow rates. Control and optimization of hydroshearing stimulation can be achieved by studying how fracture permeability evolves with shear slip and dilation. However, most experimental studies that have considered fracture slip and permeability evolution have used force-driven shear tests or have manually displaced the specimens to represent fracture slip. A few studies have considered fluid injection-driven slip but only using saw-cut smooth joints. In this work, we have conducted shear slip test by water injection on rough fractures. Water was injected into a granite sample containing a single tensile rough fracture to induce shear slip under triaxial condition. Flow rate during shear slip was measured to investigate fractures' permeability evolution. In addition, the effects of confining pressure, differential stress, and injection pressure on stress-dependent permeability of the granite fractures were characterized. We tested three separate samples using different methods. Non-shear flow tests were conducted on sample Sierra White granite sample #1 (herein after SW #1) under both hydrostatic and triaxial conditions to characterize fracture permeability. We observed a linear relationship between flow rate and injection pressure, and an exponential relationship between flow rate and confining pressure. In addition, fluid injection-driven shear tests were performed on samples SW #2 and SW #3 using constant stress mode and constant displacement mode, respectively. Shear rates observed during the constant stress test were ~10^{-3} m/s and yielded up to 3 orders of magnitude increases in flow rate while the constant displacement mode caused ~10^{-5} m/s sliding rate and 20 times increase in flow rate through the fracture.

1. INTRODUCTION

Enhanced Geothermal Systems (EGS) represent enormous renewable energy reserves (Tester et al., 2006; Brown et al., 2012). Field experiments have been carried out at sites such as Newberry, Desert Peak, Fenton Hill, Soultz-sous-Foretz and Rosemanowes. The primary objective of these field demonstrations has been to create flow paths through basement rock to facilitate heat transfer. Various stimulation mechanisms have been tested at these sites depending on the geology of the host rock, fault structures, natural fractures etc. Shear slip (Pine and Batchelor, 1984; Willis-Richards et al., 1996; Baria et al., 1999; Rahman et al., 2002; Nygren and Ghassemi, 2005; Cheng and Ghassemi, 2016) and the propagation of natural fractures are important mechanisms of permeability enhancement in EGS reservoirs (Min et al., 2010; Ghassemi, 2011; Huang et al., 2013; Jung, 2013; McClure and Horne, 2013; Kamali and Ghassemi, 2016). Often, crystalline basement rocks have pre-existing sealed fracture networks that are activated prior to the creation of new fractures since the sealing material is usually much weaker than the surrounding rock. The objective of shear stimulation is to create a stimulated volume with increased permeability to circulate large volumes of water. This is carried out at pressures below the minimum principle stress to avoid excessive fracture growth and large surface area. Fractures that are sheared tend to self-prop due to asperities.

Effective design of EGS can benefit from understanding of how the permeability of the fractures will change with injection and shear slip. However, most current experimental works have focused on force-driven fracture slip using direct shear machines (Esaki et al., 1991; Yeo et al., 1998; Esaki et al., 1999; Li et al., 2008; Park et al., 2013) or have manually displaced specimens to represent fracture slip (Duram and Bonner, 1994; Chen et al., 2000; Zhang et al., 2013; Crawford et al., 2016; Daniel et al., 2016; Hofmann et al., 2016). All results of these tests have been used to prove that it is a reliable technique to enhance permeability through inducing shear slip of fractures. However, force-driven fracture slip induced by mechanical force but not induced by fluid injection and the direct shear assembly has some disadvantages such as fractures are sheared without confining pressure, they have low normal stress capacity, and extremely low fluid injection pressure due to sealing issues. The method of using manually displaced/offset specimens cannot well simulate the fracture surface damage due to asperity cutoff and gouge production during shear sliding, and could subsequently overestimate the flow rate enhancements. A few researchers have conducted fluid-driven shear tests on saw-cut smooth fractures through injection pressure increase (Nemoto et al., 2007) or downstream/outlet pressure drop (Bauer et al., 2016). The latter demonstrated the role of pressure change and cooling on fracture slip. These works have indicated that relatively large shear sliding can be induced on smooth fractures by fluid flow, resulting in relatively small permeability enhancements (<10 times). Both flow rate measurements in the two papers were from transient flow state; steady-state flow rate should be smaller. To fully simulate the process of fluid-driven shear slip on rough fractures and the coupled permeability evolution, we carried out triaxial shear tests on rough granite fractures by increasing injection pressure to induce shear slip, and then we characterized the relationship between shear slip and permeability enhancements. Results show that two to three orders of magnitude increase in flow rate can be achieved with small shear slip (0.2 to 2 mm scale) under the triaxial shear tests of granite fractures.

During the water cycling in EGS operations, pore pressure in fractures varies under different conditions of water injection and production. In addition, confining pressure and differential stress acting on fractures also change with formation depth and operations. Therefore, stress-dependent permeability of fractures was also investigated by running non-shear flow tests under both hydrostatic and triaxial conditions. Steady-state flow rates under different stress conditions were measured in the flow tests. It was observed that flow rate tends to linearly increase with the increase of injection pressure, but tends to linearly decrease with the increase of differential stress. On the other hand, an exponential relationship was noticed between flow rate and confining pressure. Some similar stress-dependent permeability correlations were presented in previous studies (Chen et al., 2000; Zhang and Nemcik, 2013; Singh et al., 2015; Hofmann et al., 2016).

2. EXPERIMENT METHODS

2.1 Sample Preparation and Flow Path Design

Samples used in this study are Sierra White granite acquired from a commercial outlet and arrived at the laboratory in the form of cubic blocks (330mm×330mm×330mm). To create a single tensile rough fracture in granites, a cubic block of granite was firstly separated into several small rectangular pieces with dimension of 75mm×75mm×150mm, and a groove with a given inclination angle was cut on one side of the rectangular piece using a diamond saw. Then an MTS 810 frame fitted with a V-shaped blade was utilized to induce a single tensile fracture by splitting the rock. After that, a diamond coring system was used to obtain cylindrical granite cores with a single tensile fracture (Figure 1). The end surfaces of each core were finely polished using a rock surface grinder (Brown & Sharpe 818 Micromaster Grinder) according to ISRM standards. The sample dimension details are shown in Table.1. In addition, 3.175 mm diamond drill bits were used to drill holes (hole diameter is 3.5 mm) on each side of the single fracture to form flow paths to the fracture. In the test, water is injected into the facture from the bottom hole and is produced out from the top hole. The flow path and approximate dimensions are shown in Figure 2.

(a) **(b)** **(c)**

Figure 1: Sample preparation: (a) rectangular piece with groove; (b) rock splitting using V-shape blade; (c) cylindrical core.

Table 1: Dimension details of granite samples.

Sample #	Length (L), mm	Diameter (D), mm	Inclination angle (θ)	Density (ρ), g/cm^3
SW #1	99.61	55.47	43°	2.67
SW #2	116.71	55.48	36°	
SW #3	122.86	55.48	38°	

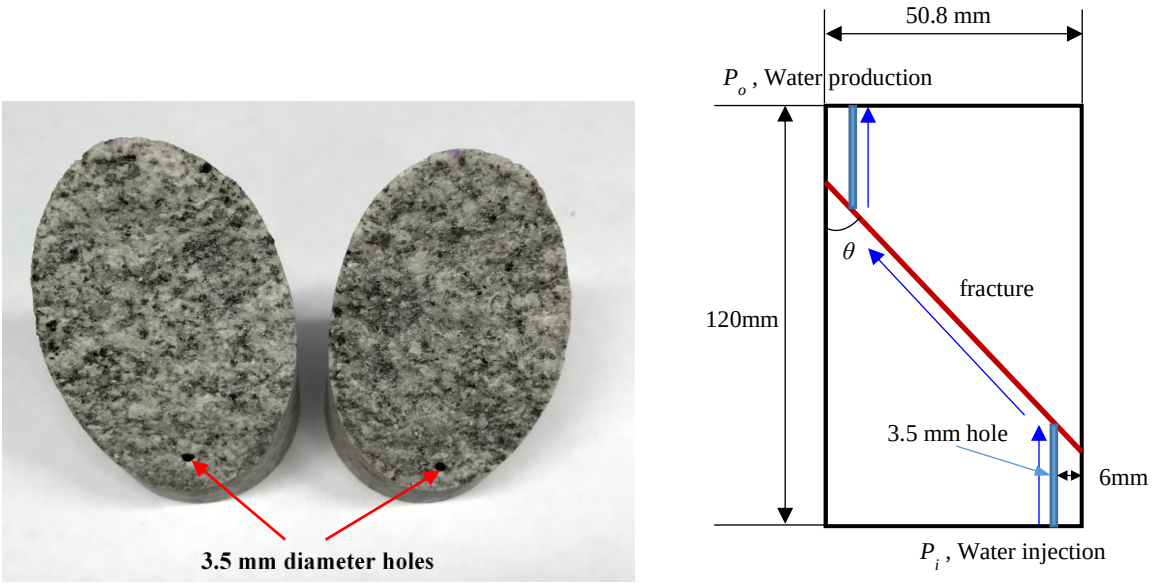

Figure 2: (a) Tensile fracked granite sample with holes; (b) the sketch of flow path and approximate dimensions.

2.2 Sample setup and flow measurements

The triaxial shear tests were carried out using an MTS 816 frame, which has a maximum 1000 kN axial load and includes a triaxial cell with 138 MPa (20,000 psi) confining pressure capacity. Control and data acquisition were performed using MTS Series 793^{TM} Control software. The setup of a cylindrical specimen with a fracture inclined at θ degree with the vertical axis is shown in Figure 3. During the triaxial test, the average axial displacement of the rock sample was measured by two Linear Variable Differential Transformer (LVDT) position sensors. Another LVDT attached on a radial ring was used to record transverse displacement. Before testing, all three LVDTs were accurately calibrated to control the average error below 0.01 mm.

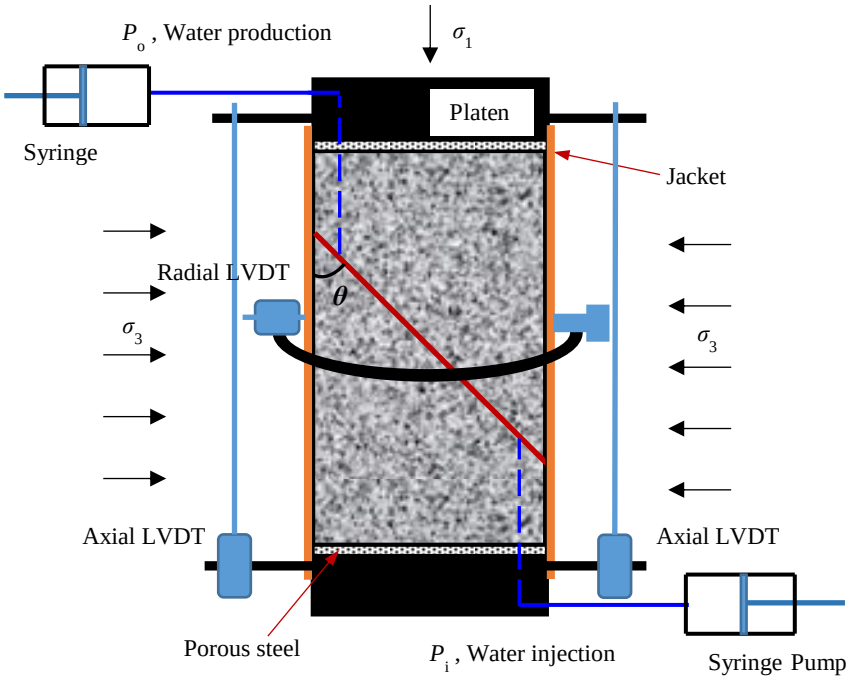

Figure 3: Sketch of sample setup and LVDTs configuration.

Two Teledyne ISCO D-Series syringe pumps (maximum 68.95 MPa pressure limit and 103 mL volume capacity) were used to control fluid flow and measure flow parameters. An open source software "Disco" provided by Los Alamos National Laboratory was used to perform pump operation and data acquisition. The sketch of fluid flow is illustrated in Figure 4 showing that water was injected into the

fracture by pump A and then produced by pump B. During the test, the flow parameters including pressure, water volume, and flow rate of each pumping operation were measured.

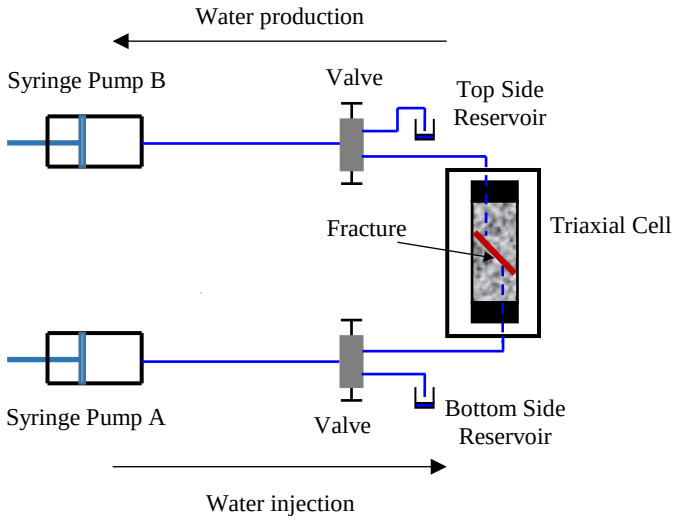

Figure 4: Water flow design and flow measurements.

2.3 Experiment procedure

In this study, we focus on two main issues: stress-dependent permeability characterization and permeability evolution in response to injection-driven shear slip. Therefore, several flow and shear tests were carried out on fractures in granite cores.

2.3.1 Stress-dependent permeability test

To address permeability change with stress, non-shear slip flow tests were conducted on fractured granite SW #1 under both hydrostatic and triaxial conditions. In the hydrostatic flow test, we measured flow parameters of fractured granite SW #1 under different values of confining pressure and injection pressure (Table. 2). Hydraulic oil in the triaxial cell was used to apply confining pressure (σ_3) controlled by an MTS Model 286.20 Confining Pressure Intensifier, which has an inside pressure transducer to measure pressure magnitudes. Once the fractured granite sample was subjected to a target confining pressure, water was injected into the bottom of the sample by syringe pump A and collected by syringe pump B which connected to the top of the sample. Under each confining pressure stage, the production pressure (P_o) was kept equal to atmospheric pressure while the injection pressure (P_i) was increased with a constant pressure rate (0.03 MPa/s), and then water was circulated from pump A to pump B due to the pressure difference between the two pumps. Each pressure stage lasted 300 seconds including the pressure buildup which required 60-120 seconds. After the target pressure was achieved, we waited 120 seconds before recording the flow rates to ensure steady-state flow had been reached. When we observed the flow rate out of pump A to be near identical to the flow rate into pump B we considered flow through the fractured sample to have reached a steady-state flow regime.

Table 2: Hydrostatic flow tests under different values of confining pressure and injection pressure.

	Confining pressure (σ_3), MPa					Differential Stress ($\sigma_1 - \sigma_3$), MPa	Production pressure (P_o), MPa
	5	10	20	30	40		
Injection pressure (P_i), MPa	1	1	1	1	1	0	0
	2	2	2	2	2		
	2.5	4	4	4	4		
	3	5	6	6	6		
	3.5	6	8	8	8		
	4	7	10	10	12		
		8	12	12	16		
			14	14	18		
			16	16	20		
			18	18	24		
				20	26		
				24	28		
				26	32		
				28	34		
					38		

After the hydrostatic flow test, we continued to run a non-shear triaxial flow test on fractured granite sample SW #1 to characterize the effect of differential stress ($\sigma_1 - \sigma_3$) on permeability / flow rates. The confining pressure (σ_3) and the flow outlet pressure (P_o) were kept constant at 30 MPa and 5 MPa, respectively. Then we conducted flow tests by increasing the injection pressure under four different differential stress stages: 20 MPa, 40 MPa, 60 MPa and 80 MPa. Steady-state flow parameters were measured under several different levels of injection / flow inlet pressure (P_i) for each differential stress stage (Table. 3). Since the differential stresses used in the test were smaller than the critical shear strength, significant shear slip wasn't induced during the triaxial flow tests of sample SW #1.

Table 3: Triaxial flow tests under different values of differential stress and injection pressure.

	Differential Stress ($\sigma_1 - \sigma_3$), MPa				Confining pressure (σ_3), MPa	Production pressure (P_o), MPa
	20	40	60	80		
Injection pressure (P_i), MPa	8	8	8	8	30	5
	12	12	12	12		
	15	15	15	15		
	18	18	18	18		
	20	20	20	20		
	22	22	22	22		
	26	26	26	26		
	28	28	28	28		

2.3.2 Injection-driven shear test

The aperture of rough fractures can be increased by inducing dilatant shear slip through water injection, which has been recognized as a dominant mechanism of permeability enhancement during hydraulic stimulation of engineered geothermal systems (EGS). In our fluid injection-driven shear tests, we induced fracture slip by increasing water injection pressure. To compare the fracture slip rate, shear displacement, gouge production and fracture surface damage, we conducted two shear tests under different control modes: One test used constant stress control on fractured granite sample SW #2; the other test was carried out using constant displacement control for fractured granite sample SW #3. For both shear tests, we controlled the confining pressure and flow outlet / production pressure as constants to be 30 MPa and 5 MPa, respectively. The flow inlet /injection pressure was selected to be 5 MPa initially, but later was increased incrementally to induce fracture slip. Before running shear tests, common triaxial tests were conducted on both fractured specimens under initial conditions ($\sigma_3 = 30$ Mpa, $P_o = P_o = 5$ MPa) until the dilation point or critical strength of the fracture was determined from stress-strain curves. The objectives of this step are stably closing the fresh open tensile fracture and providing the reference critical shear strength value for the shear tests.

In the test with constant stress control mode, we loaded the sample SW #2 at a constant stress rate 5 MPa / min to 120 MPa differential stress level under the same initial conditions ($\sigma_3 = 30$ MPa, $P_o = P_o = 5$ MPa), and controlled the differential stress as a constant 120 MPa during the whole shear test of sample SW #2. However, in the test with constant displacement control mode, the sample SW #3 was loaded with a constant displacement rate of 0.01 mm/min to 180 MPa differential stress level under initial conditions and then the displacement was controlled as constant which means the load piston of the frame cannot move during the test. Once the values of stress, LVDTs and flow rates in syringe pumps are stable under each test with different control modes, the injection pressure was stepwise increased to induce shear slip while confining pressure and flow outlet pressure were kept constants.

3. EXPERIMENT RESULTS

3.1 Hydrostatic flow test

For the hydrostatic test of sample SW #1, the measured flow rate (Q) versus injection pressure (P_i) under different confining pressures (from 5 to 40 MPa) have been plotted in Figure 5. It can be observed that flow rate linearly rises with the increase of injection pressure under each confining pressure stage. However, under relatively high injection pressure, some flow rate data are larger and deviate from the linear relationship. In such cases, the difference between the confining pressure and the injection pressure are less than 4 MPa, so that the effective stress is low. The relationship between flow rate and confining pressure, corresponding to different injection pressures (P_i = 1, 2, 4, 6, and 8 MPa), are shown in Figure 6. The significant reduction of flow rate with the increase of confining pressure can be noticed from the plot. An approximate exponential relationship can be obtained using a regression technique. The flow rates measured under each combination of injection pressure and confining pressure are listed in Table 4. A notable phenomenon we identified is the character of the exponential curves for the flow rate versus confining pressure. The multiplier of the exponent was -0.07 and the same for all cases analyzed in this test, however, the coefficient changed for various injection pressures (Figure 6). We noticed the same behavior in our previous tests and believe that the multiplier in the exponent is fracture specific and related to the geometry and roughness while the coefficient seems to be stress dependent.

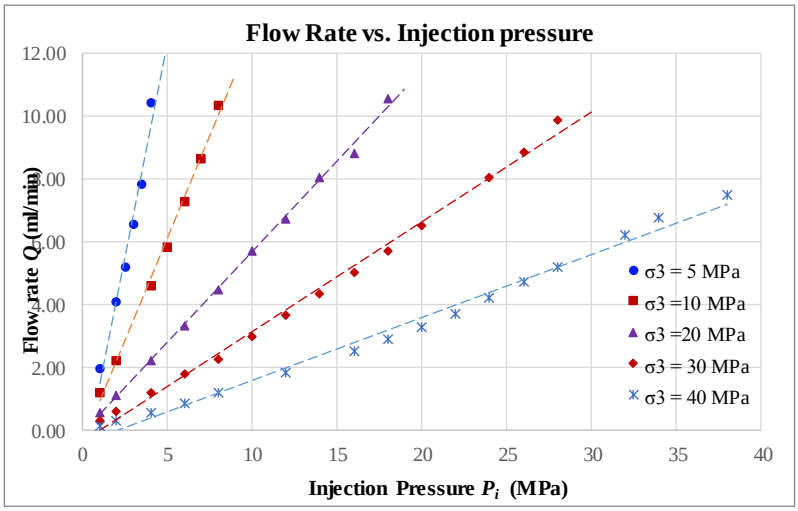

Figure 5: Flow rate versus injection pressure under hydrostatic flow test.

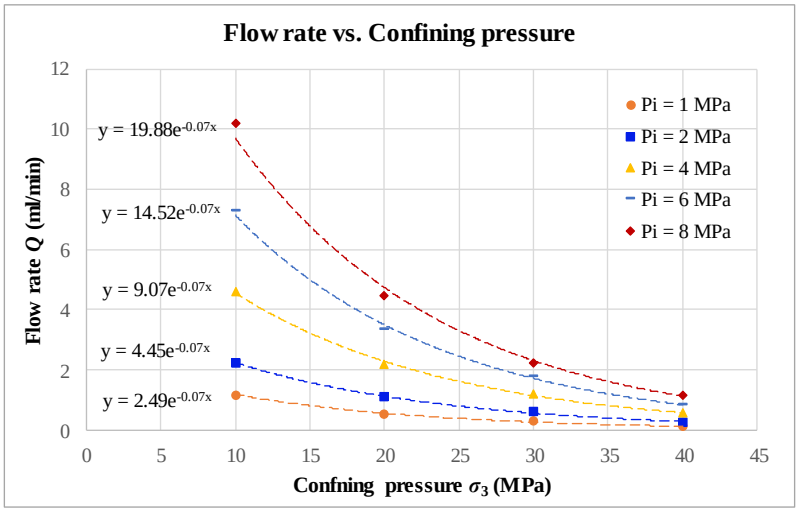

Figure 6: Flow rate versus confining pressure under hydrostatic flow test.

Table 4: Flow rate measurements of hydrostatic flow test.

σ_3 MPa	P_i MPa	Q ml/min	σ_3 MPa	P_i MPa	Q ml/min	σ_3 MPa	P_i MPa	Q ml/min	σ_3 MPa	P_i MPa	Q ml/min	σ_3 MPa	P MPa	Q ml/min
5	1	1.95	10	1	1.17	20	1	0.55	30	1	0.29	40	1	0.12
	2	4.07		2	2.23		2	1.10		2	0.60		2	0.27
	2.5	5.17		4	4.60		4	2.20		4	1.20		4	0.57
	3	6.55		5	5.83		6	3.33		6	1.79		6	0.84
	3.5	7.81		6	7.28		8	4.48		8	2.24		8	1.17
	4	10.42		7	8.62		10	5.70		10	2.99		12	1.81
				8	10.36		12	6.72		12	3.66		16	2.50
							14	8.03		14	4.33		18	2.89
							16	8.81		16	5.01		20	3.29
							18	10.57		18	5.72		22	3.71
										20	6.52		24	4.20
										24	8.05		26	4.71
										26	8.85		28	5.18
										28	9.89		32	6.23
													34	6.78
													38	7.49

3.2 Triaxial flow test under deviatoric loading

The flow rate measurements of triaxial flow test are shown in Table 5. The relationship between flow rate (Q) and differential stress ($\sigma_1 - \sigma_3$) under various injection pressures (P_i = 8, 12, 15, 18, 20, 22, 26 and 28 MPa) have been plotted in Figure 7. Flow rate tends to linearly decrease with the increase of differential stress, with a slight departure from this trend for the cases with high injection pressures (26 and 28 MPa) which are close to the 30 MPa confining pressure (and thus low effective stress).

Table 5: Flow rate measurements of triaxial flow test.

$\sigma_1 - \sigma_3$ MPa	P_i MPa	Q ml/min	$\sigma_1 - \sigma_3$ MPa	P_i MPa	Q ml/min	$\sigma_1 - \sigma_3$ MPa	P_i MPa	Q ml/min	$\sigma_1 - \sigma_3$ MPa	P_i MPa	Q ml/min
20	8	0.21	40	8	0.17	60	8	0.13	80	8	0.11
	12	0.50		12	0.40		12	0.31		12	0.21
	15	0.74		15	0.59		15	0.45		15	0.28
	18	1.02		18	0.81		18	0.61		18	0.37
	20	1.24		20	0.96		20	0.72		20	0.43
	22	1.48		22	1.14		22	0.85		22	0.51
	26	2.17		26	1.59		26	1.19		26	0.73
	28	2.68		28	1.90		28	1.42		28	0.94

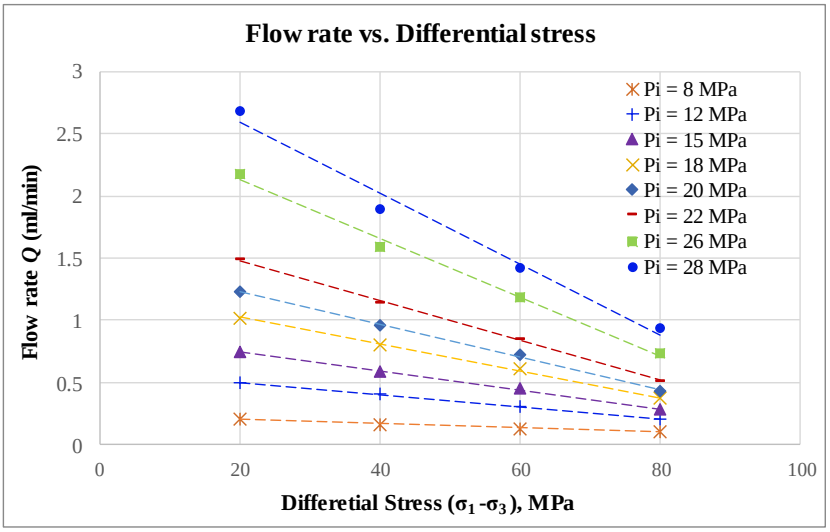

Figure 7: Flow rate versus differential stress under triaxial flow test.

3.3 Injection-driven shear test

3.3.1 Constant stress control mode

As described above, a triaxial shear test was conducted on fractured granite sample SW #2 with constant stress control mode which means the differential stress was kept constant ($\sigma_1 - \sigma_3$ =120 MPa) during the water injection process. Under this stress control mode, the displacement of the loading piston in MTS 816 frame will increase to provide more compression and compensate for the stress drop due to fracture slip. In addition, the frictional resistance in the fracture gradually decreases with the increase of fracture sliding. Therefore, once sliding is initiated the fracture will continue sliding until the piston movement triggers the displacement limit. Similar to the stress-dependent permeability test we increased the injection pressure step-wise at a rate of 0.03 MPa/s. Once each injection pressure target was reached, we waited 120 seconds before collecting the representative steady-state flow data. Flow rates under several different injection pressures (P_i = 8, 12, 15, 18, 20, 22, 24 and 26 MPa) were measured and listed in Table 6. A similar linear relationship between flow rate and injection pressure was observed under the first several low injection pressure stages. The sample began to slide rapidly at around 26 MPa injection pressure accompanied by audible cracking, and a large sliding (> 2 mm) was induced with a correspondingly large flow rate increase to about 11.40 ml/min (Figure 8). Unfortunately, the jacket confining the sample is only capable of sustaining a few millimeters of sliding and burst prior to steady-state flow being achieved. However, such a large transient flow is very intriguing. Transient flows during previous sliding stages in the same test and subsequent tests never exceeded the steady-state flow by more than 2 or 3 times. Therefore, an increase in flow rate up to three orders of magnitude can be expected from this triaxial shear test under the constant stress control mode. In addition, the calculated average fracture slip rate was approximately 4×10^{-3} m/s.

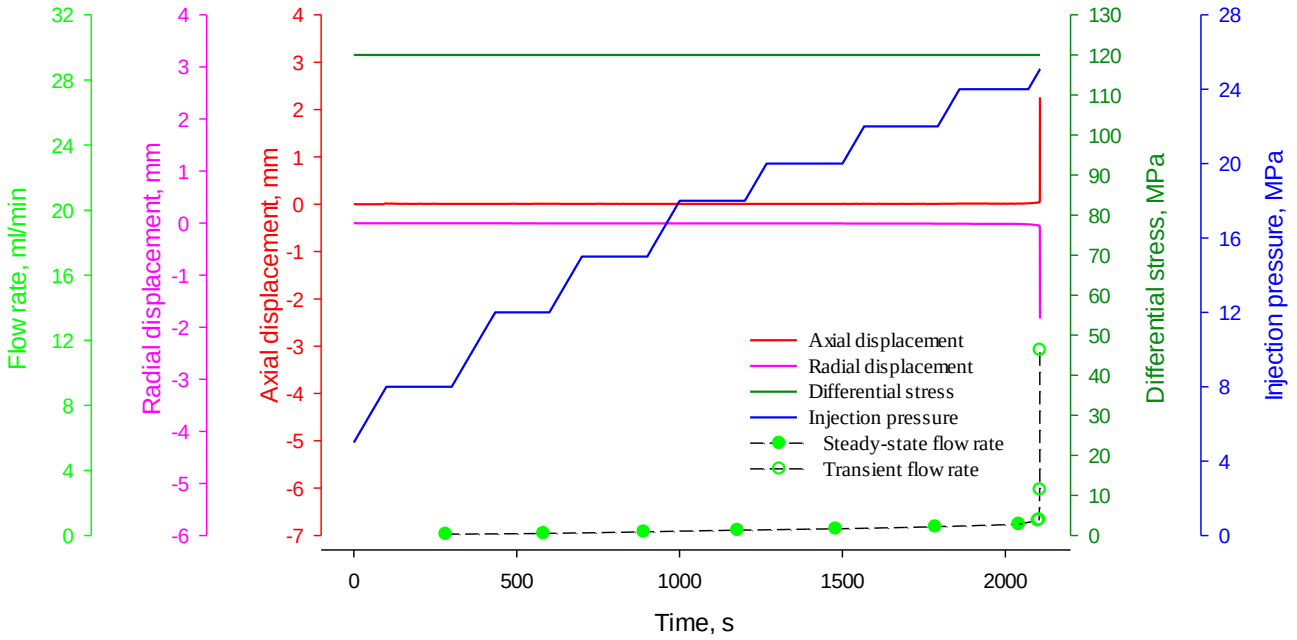

Figure 8: Injection-driven shear test using constant stress control mode.

Table 6: Flow rate measurements of injection-driven shear test on sample SW #2.

$\sigma_1 - \sigma_3$ MPa	P_i MPa	Q ml/min	Flow regime
120	8	0.08	Steady-state flow
	12	0.12	
	15	0.22	
	18	0.32	
	20	0.41	
	22	0.54	
	24	0.69	
	26	0.97	Transient flow
		2.81	
		11.40	

3.3.2 Constant displacement control mode

The constant displacement control mode was used to conduct triaxial shear test for sample SW #3, which means the piston displacement of MTS frame was kept constant during the triaxial shear test. Under this displacement control mode, the differential stress acting on the sample decreases significantly once shear slip of the fracture is initiated since the compression exerted on the sample by the piston drops with the gradual sliding of the fracture. As a result, the fracture sliding will interlock at some point after the differential stress decreases to a low level. In this test, relatively small radial displacement (< 0.3 mm) was induced during the 29 MPa injection stage. The measurements of axial displacement, radial displacement, differential stress, stepwise increased injection pressure and steady-state flow rate have been analyzed as shown in Figure 9. In this test, only four injection pressure stages were used to induce sliding; 16 MPa, 20 MPa, 24 MPa and 29 MPa. A gradual increase of both radial displacement and flow rate with the stepwise increase of injection pressure can be noticed in the plot, while the differential stress decreased with the increase of injection pressure. At the last injection stage, a sudden shear slip on sample SW #3 was also induced and flow rate was enhanced to 1.03 ml/min (Table 7) which was an increase of around 20 times compared to the base flow rate of 0.05 ml/min. Also, it is observed that a linear relationship between flow rate and injection pressure existed before shear slip, which means the linear increase of flow rate was because of the fracture aperture dilation due to injection pressure but was not related to the shear slip. We observed 0.26 mm radial dilation while axial displacement remained relatively low in comparison. The average fracture slip rate of the shear test on sample SW #3 is around 2×10^{-5} m/s, which is two order of magnitudes smaller than the slip rate of sample SW #2. In addition, the differential stress of sample SW #3 suddenly dropped from 160 MPa to 50 MPa while the differential stress was kept constant during the shear test of SW #2.

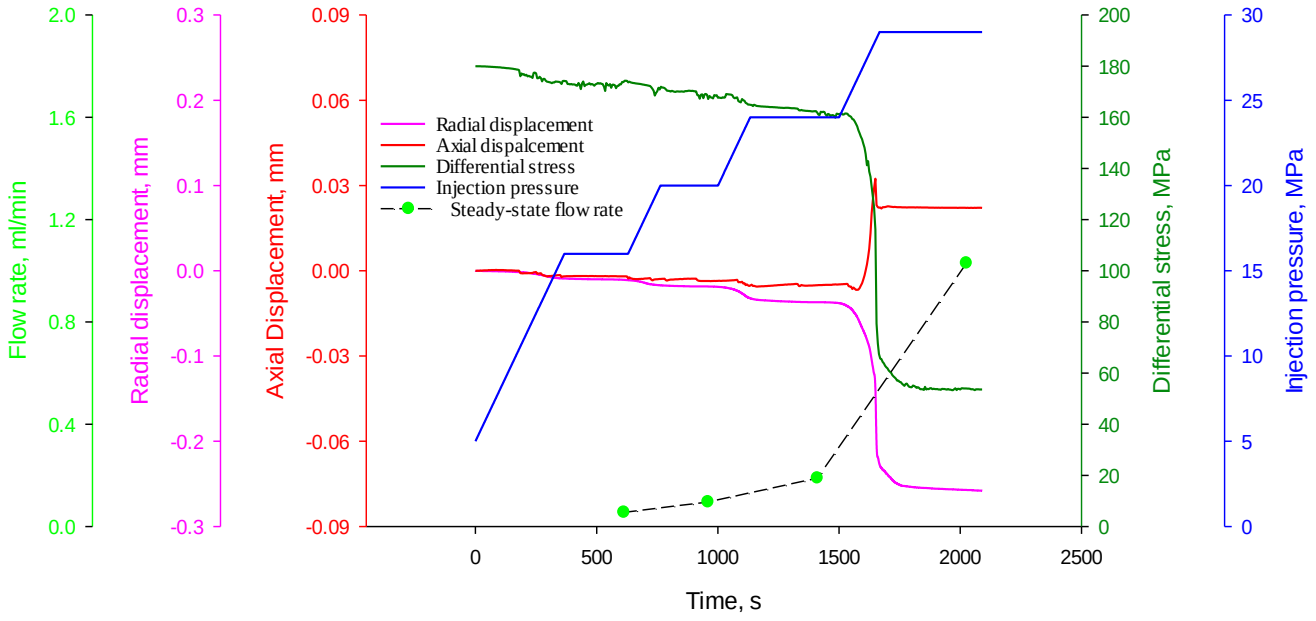

Figure 9: Fluid injection-driven shear test using constant displacement control mode.

Table 7: Flow rate measurements of injection-driven shear test on sample SW #3.

P_i MPa	Q ml/min	Flow regime
16	0.05	Steady-state flow
20	0.10	
24	0.19	
29	1.03	

4. DISCUSSION

4.1 Permeability evolution and hysteresis

For both shear tests on samples SW #2 and SW #3, an increase of two to three orders of magnitude in flow rate was observed during the process of fracture shear slip. Based on the comparison of the displacement of the two samples, we noticed that flow rate tends to increase with the increase of shear slip displacement. Sample SW #2 showed a higher flow rate change due to the larger shear slip displacement. In addition, we also observed that large fracture slip always was initiated at the pressure build-up stage (transient flow regime). Under steady-state flow conditions, there is no longer pressure buildup in the fracture which caused the slip rate to decrease significantly compared to the slip rate during transient flow.

The injection pressure was decreased stepwise after the shear slip occurred in sample SW #3, and flow rates in the path of injection pressure unloading also were measured as shown in Table 8. A remarkable permeability hysteresis feature was recognized on sample SW #3 based on the flow rate measurements of the increase-decrease cycle of injection pressure (Figure 10). Once high flow rates were observed at 29 MPa injection pressure (Table 8), flow rate increase was preserved while the injection pressure was stepwise decreased along the same path down to 16 MPa. A probable explanation for this is that the last injection stage caused enough dilation to allow the fracture to permanently prop open due to the asperities.

Table 8: Flow rate measurements of cyclical injection pressure on sample SW #3.

Loading		Unloading	
P_i MPa	Q ml/min	P_i MPa	Q ml/min
16	0.05	24	0.65
20	0.10	20	0.45
24	0.19	16	0.30
29	1.03		

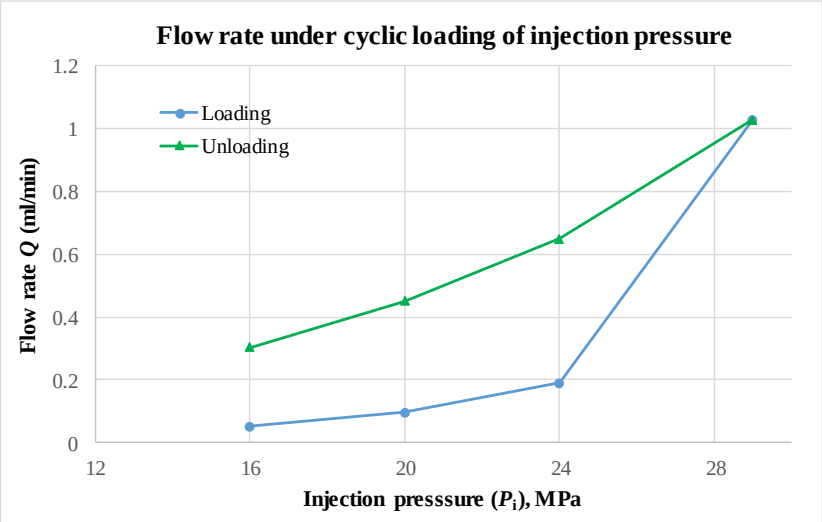

Figure 10: Permeability/flow rate hysteresis under cyclic loading of injection pressure.

4.2 Surface damage and gouge production

After the shear slip were induced during the tests, significant surface damage was observed on both samples (Figure 11). Large amounts of fine gouge and visible surface damage can be observed on sample SW #2 due to the complete cutoff of asperities by fracture shear slip. On the other hand, it is noticed that only small amounts of gouge were produced on sample SW #3 which means the surface damage induced by the shear slip is relatively small. This observation correlates well with the different amount of slip displacement between the two samples. The fine gouge (it is finer than the grain size of granite) observed was perhaps because of large shear slip which caused asperity rupture once contact stress overcame asperity strength (Daniel et al., 2016).

Figure 11: Gouge production and slickensides on tested samples SW #2 and SW #3.

4.3 Experimental sliding rate

The constant stress test was applied because shear rates of earthquakes are typically about 1m/s, thus the faster shear rate likely better represents in-situ conditions. However, this method fails to capture the relaxation of the stresses responsible for the sliding. Therefore, the constant displacement test was conducted to capture the phenomenon of stress relaxation after slip which occurs on faults and fractures. Guglielmi et al. (2015) directly measured shear slip on a fault during a field-scale injection test and observed ~ 10^{-6} to ~ 10^{-5} m/s slip rates at the onset of micro-seismicity. Our injection-driven laboratory shear tests achieved similar slip rates.

5. CONCLUSION

Three granite samples with a single tensile rough fracture were used to conduct fluid flow and shear tests to characterize stress-dependent permeability and study the relationship between permeability evolution and shear slip. The flow rates measured during the non-shear flow tests yielded linear relationships with injection pressure and differential stress and an exponential relationship with confining pressure. In the constant stress and constant displacement shear tests sliding was successfully induced by injecting water into the fracture which subsequently caused large increases in permeability. Sliding observed was in the range of 0.2 – 2 mm and sliding rates were ~10^{-5} m/s and ~10^{-3} m/s in the constant displacement and constant stress tests, respectively. These sliding rates, though slow, are on the same order of magnitude as those recorded by Guglielmi et al. (2015) in a field injection test on a natural fault. Though our constant stress test was unable to achieve steady-state flow at 26 MPa injection pressure, the large increase in transient flow rate is highly indicative of similarly large permeability increases. The constant displacement test yielded definitive increase in steady-state flow rate by a factor of 20 from the base pressure measurement at 8 MPa. Gouge production was also notably higher in the constant stress test in which large sliding occurred while minimal damage was observed on the fracture surface subjected to the constant displacement test. Further study into the relationship between fracture roughness, gouge production and permeability enhancement would be extremely beneficial. These results clearly indicate that shear stimulation can be used to engineer geothermal systems.

REFERENCES

Baria, R., et al.: HDR/HWR reservoirs: concepts, understanding and creation. *Geothermics*, 1999. 28(4): p. 533-552.

Bauer, S., et al.: Experimental and Numerical Investigation of Hydro-Thermally Induced Shear Stimulation. in *50th US Rock Mechanics/Geomechanics Symposium*. 2016. American Rock Mechanics Association.

Brown, D.W., et al.: Mining the Earth's Heat: Hot Dry Rock Geothermal Energy. 2012: Springer Berlin Heidelberg.

Chen, Z., et al.: An experimental investigation of hydraulic behaviour of fractures and joints in granitic rock. *International Journal of Rock Mechanics and Mining Sciences*, 2000. 37(7): p. 1061-1071.

Cheng, Q. and A. Ghassemi: Numerical Modeling of Newberry Egs Stimulation. 2016, American Rock Mechanics Association.

Crawford, B.R., et al.: Incorporating Universal Scaling of Fracture Stiffness and Surface Roughness Effects for Improved Productivity Prediction in Naturally Fractured Reservoirs. 2016, American Rock Mechanics Association.

Durham, W. and B. Bonner: Self-propping and fluid flow in slightly offset joints at high effective pressures. *Journal of Geophysical Research: Solid Earth*, 1994. 99(B5): p. 9391-9399.

Esaki, T., et al.: Development of a shear-flow test apparatus and determination of coupled properties for a single rock joint. *International Journal of Rock Mechanics and Mining Sciences*, 1999. 36(5): p. 641-650.

Esaki, T., et al.: Shear-flow Coupling Test On Rock Joints. 1991, International Society for Rock Mechanics.

Ghassemi, 2011. Three-dimensional Modeling of Fracture Clusters in Geothermal Reservoirs. *Geothermal Technologies Program 2011 Peer Review*. EGS Component R&D Stimulation Prediction Models.

Guglielmi, Y., et al.: Seismicity triggered by fluid injection–induced aseismic slip. *Science*, 2015. 348(6240): p. 1224-1226.

Hofmann, H., et al.: Transmissivity of aligned and displaced tensile fractures in granitic rocks during cyclic loading. *International Journal of Rock Mechanics and Mining Sciences*, 2016. 87: p. 69-84.

Huang, K., Z. Zhang, and A. Ghassemi: Modeling three-dimensional hydraulic fracture propagation using virtual multidimensional internal bonds. *International Journal for Numerical and Analytical Methods in Geomechanics*, 2013. 37(13): p. 2021-2038.

Jung, R.: EGS — Goodbye or Back to the Future 95. *Effective and Sustainable Hydraulic Fracturing*. 2013.

Kamali, A. and A. Ghassemi: Analysis of Natural Fracture Shear Slip and Propagation in Response to Injection. 2016. Stanford Geothermal Workshop. Stanford, California, February 22nd–25th.

Li, B., et al.: Experimental study of the hydro-mechanical behavior of rock joints using a parallel-plate model containing contact areas and artificial fractures. *International Journal of Rock Mechanics and Mining Sciences*, 2008. 45(3): p. 362-375.

McClure, M. and R. Horne: Conditions required for shear stimulation in EGS. in *Proceedings of the 2013 European Geothermal Congress, Pisa, Italy*. 2013.

Min, K.S., Z. Zhang, and A. Ghassemi: Numerical Analysis of Multiple Fracture Propagation In Heterogeneous Rock. 2010, American Rock Mechanics Association.

Nemoto, K., et al.: Mechanical and hydraulic coupling of injection-induced slip along pre-existing fractures. *Geothermics*, 2008. 37(2): p. 157-172.

Nygren, A. and A. Ghassemi: Influence of Cold Water Injection on Critically Stressed Fractures in Coso Geothermal Field, *CA*. 2005, American Rock Mechanics Association.

Olsson, W. and S. Brown: Hydromechanical response of a fracture undergoing compression and shear. *International journal of rock mechanics and mining sciences & geomechanics abstracts*. 1993. Elsevier.

Park, H., et al.: Development of coupled shear-flow-visualization apparatus and data analysis. *International Journal of Rock Mechanics and Mining Sciences*, 2013. 63: p. 72-81.

Pine, R.J. and A.S. Batchelor: Downward migration of shearing in jointed rock during hydraulic injections. *International Journal of Rock Mechanics and Mining Sciences*, 1984. 21(5): p. 249-263.

Rahman, M.K., M.M. Hossain, and S.S. Rahman: A shear-dilation-based model for evaluation of hydraulically stimulated naturally fractured reservoirs. *International Journal for Numerical and Analytical Methods in Geomechanics*, 2002. 26(5): p. 469-497.

Singh, K., D. Singh, and P. Ranjith: Laboratory simulation of flow through single fractured granite. *Rock Mechanics and Rock Engineering*, 2015. 48(3): p. 987-1000.

Tester et al.: The Future of Geothermal Energy: Impact of Enhanced Geothermal Systems (EGS) on the United States in the 21st Century: an Assessment. 2006: Massachusetts Institute of Technology.

Vogler, D., et al.: Permeability Evolution in Natural Fractures Subject to Cyclic Loading and Gouge Formation. *Rock Mechanics and Rock Engineering*, 2016. 49(9): p. 3463-3479.

Willis-Richards, J., K. Watanabe, and H. Takahashi: Progress toward a stochastic rock mechanics model of engineered geothermal systems. *Journal of Geophysical Research: Solid Earth*, 1996. 101(B8): p. 17481-17496.

Yeo, I., M. De Freitas, and R. Zimmerman: Effect of shear displacement on the aperture and permeability of a rock fracture. *International Journal of Rock Mechanics and Mining Sciences*, 1998. 35(8): p. 1051-1070.

Zhang, Z. and J. Nemcik: Friction factor of water flow through rough rock fractures. *Rock mechanics and rock engineering*, 2013. 46(5): p. 1125-1134.

Zhang, Z., J. Nemcik, and S. Ma: Micro-and macro-behaviour of fluid flow through rock fractures: an experimental study. *Hydrogeology Journal*, 2013. 21(8): p. 1717-1729.